The Journal of Infectious Diseases

MAJOR ARTICLE

Cathepsin K Contributes to Cavitation and Collagen Turnover in Pulmonary Tuberculosis

Andre Kubler,[1,3,a] Christer Larsson,[7,a] Brian Luna,[3,a] Bruno B. Andrade,[5] Eduardo P. Amaral,[5] Michael Urbanowski,[3] Marlene Orandle,[6] Kevin Bock,[6] Nicole C. Ammerman,[3] Laurene S. Cheung,[3] Kathryn Winglee,[3] Marc Halushka,[4] Jin Kyun Park,[8] Alan Sher,[5] Jon S. Friedland,[1,b] Paul T. Elkington,[1,2,b] and William R. Bishai[3,b]

[1]Infectious Diseases and Immunity, Imperial College London, and [2]Faculty of Medicine, University of Southampton, United Kingdom; [3]Center for Tuberculosis Research and [4]Department of Pathology, Johns Hopkins University School of Medicine, Baltimore, [5]Immunobiology Section, Laboratory of Parasitic Diseases, and [6]Infectious Diseases Pathogenesis Section, Comparative Medicine Branch, National Institutes of Allergy and Infectious Disease, National Institutes of Health, Bethesda, Maryland; [7]Department of Molecular Biology, Umeå University, Sweden; and [8]Division of Rheumatology, Department of Internal Medicine, Seoul National University Hospital, South Korea

Cavitation in tuberculosis enables highly efficient person-to-person aerosol transmission. We performed transcriptomics in the rabbit cavitary tuberculosis model. Among 17 318 transcripts, we identified 22 upregulated proteases. Five type I collagenases were overrepresented: cathepsin K (CTSK), mast cell chymase-1 (CMA1), matrix metalloproteinase 1 (MMP-1), MMP-13, and MMP-14. Studies of collagen turnover markers, specifically, collagen type I C-terminal propeptide (CICP), urinary deoxypyridinoline (DPD), and urinary helical peptide, revealed that cavitation in tuberculosis leads to both type I collagen destruction and synthesis and that proteases other than MMP-1, MMP-13, and MMP-14 are involved, suggesting a key role for CTSK. We confirmed the importance of CTSK upregulation in human lung specimens, using immunohistochemical analysis, which revealed perigranulomatous staining for CTSK, and we showed that CTSK levels were increased in the serum of patients with tuberculosis, compared with those in controls (3.3 vs 0.3 ng/mL; $P = .005$).

Keywords. tuberculosis; cathepsin K; rabbit; collagen; collagenolysis; RNAseq.

Tuberculosis is a common, debilitating infectious disease that, if left untreated, has a fatality rate of >50% [1]. Extensively drug-resistant tuberculosis accounts for 9% of the 300 000 multidrug-resistant tuberculosis cases and costs on average $554 000 per patient to treat [2]. Tuberculosis transmission is increased by cavitary disease, which contributes to antibiotic failure and the emergence of antibiotic resistance [3–5]. Bilateral cavity formation is the most significant predictor of treatment failure for extensively drug-resistant tuberculosis [6].

Cavity formation is rarely studied, partly because it is so difficult to recreate under controlled conditions. Our current understanding is therefore derived from observational studies of human specimens, in which the histopathological hallmarks are caseous, liquefactive, and coagulative necrosis [7, 8]. The mechanisms of these processes remain elusive.

Several theories attempt to explain cavity formation. The most widely taught is that maturing granulomas invade the airway, spilling their necrotic debris and leaving a cavity at the granuloma site [9, 10]. This ignores the observation that cavities occur in a number of nongranulomatous conditions and are encountered less frequently in nontuberculous granulomatous conditions than during tuberculosis [11]. Additionally, it is known that pneumonic change is the most common pathology associated with postprimary tuberculosis in humans [12]. Other, less commonly accepted theories of cavitation include cystic dilation, infarction, postobstructive pneumonia, and postobstructive increases in intra-alveolar pressure [11].

In this study, we use our ability to manipulate cavity formation to explore effectors of cavity formation in a rabbit model of postprimary tuberculosis [13]. Next-generation transcriptional profiling with RNAseq in a number of pathologies revealed that collagen-degrading proteases were among the most highly transcribed genes in cavitary disease. This is significant, as the key structural components of lung extracellular matrix (ECM) are the fibrillar collagens (type I and type III) [14], and only 9 enzymes are known to cleave the two alpha components of type I collagen, and only matrix metalloproteinase 1 (MMP-1), MMP-8, MMP-13, MMP-14, and cathepsin K (CTSK) can cleave the mature triple helical form [14–17].

We discovered that CTSK, a serine protease with the unique ability to cleave type I collagen both inside and outside its helical region [17], was strongly associated with tuberculosis pathology and that changes in collagen-breakdown products suggestive of CTSK activity were unique to rabbits in which active cavitation was taking place. Finally, we demonstrated that CTSK expression is associated with human immunopathology

Received 17 June 2015; accepted 31 August 2015; published online 27 September 2015.
Presented in part: 9th International Conference on the Pathogenesis of Mycobacterial Infections, Stockholm, Sweden, 26–29 June 2014.
[a]A. K., C. L., and B. L. contributed equally to this work.
[b]J. S. F., P. T. E., and W. R. B. contributed equally to this work.
Correspondence: W. R. Bishai, Johns Hopkins School of Medicine, 1550 Orleans St CRB2, Rm 108, Baltimore, MD 21287 (wbishai@jhmi.edu).

The Journal of Infectious Diseases® 2016;213:618–27

DOI: 10.1093/infdis/jiv458

and that an increased level of plasma CTSK is a feature of active pulmonary tuberculosis. Together, these findings suggest that collagen degradation mediated by CTSK plays an important role in cavity formation, adding to a growing body of evidence that collagen destruction is the key mechanism underlying cavity formation.

MATERIALS AND METHODS

Animal Procedures

Female New Zealand white rabbits, weighing 3–3.5 kg (Covance Research Products, Gaithersburg, Maryland), were sensitized with five 0.2-mL subcutaneous injections of 1×10^7 (lower dose) or 1×10^8 (higher dose) heat-killed *Mycobacterium bovis*, emulsified 1:1 in Freund's adjuvant. Twenty-one days after sensitization, skin test reactivity was determined by injection of 5 IU of purified protein derivative (Tubersol; Sanofi-Aventis, Bridgewater, New Jersey) and measured at 48 hours. Animals were maintained in biosafety level 3 conditions in accordance with protocols (RB11M466) approved by the Institutional Animal Care and Use Committee at Johns Hopkins University (Baltimore, Maryland). Serum/plasma specimens were collected from the central ear artery, and urine samples were obtained by bladder pressure; all specimens were collected after animals were anesthetized.

Rabbit Infection

Rabbits were anesthetized by intramuscular administration of ketamine (10 mg/kg) and xylazine (20 mg/kg) prior to endotracheal tube intubation. A 3.0-mm flexible Pentax FB-8V pediatric bronchoscope (Pentax, Montvale, New Jersey) was guided into 1 lower lobe, and 400 μL of 7.5×10^3 (lower dose) or 1×10^4 (higher dose) log-phase *Mycobacterium tuberculosis* strain H37Rv was inoculated via catheter.

Rabbit Imaging

Computed tomography and positron emission tomography (CT/PET) were performed at times specified in Supplementary Figure 1. Anesthetized animals were administered 0.2mCu 2-deoxy-2-(^{18}F)fluoro-D-glucose (^{18}F-FDG) by intravenous injection. The animal was placed in an air-tight, HEPA-filtered cylinder, and anesthesia was switched to isoflurane and oxygen. PET/CT was performed using a clinical 8-slice CT scanner (CereTom) and a Philips Mosaic HP Small Animal PET Imager. CT and PET images were coregistered using Amira (Visualization Sciences Group, Burlington, Massachusetts). Amira was also used to calculate the mean and maximum standard uptake values in rabbit lungs.

Rabbit Immune Suppression and Reconstitution

At 140 days after infection, rabbits were administered 10 mg/kg dexamethasone and then continuation dose of 0.1 mg/kg/day for 27 days as described in a previous protocol [18].

Necropsy and Tissue Samples

Rabbits were euthanized following anesthesia by intravenous injection of Euthasol (Virbac, Fort Worth, Texas). Tissues for RNAseq analysis were transferred to RNA*later* (Ambion, Life technologies, Grand Island, New York) within 10 minutes. Tissue for protein analysis was snap frozen in liquid nitrogen. Samples for histological analysis were fixed in 10% formalin or in phosphate-buffered saline (PBS) for enumeration of colony-forming units.

RNA Preparation

After 24 hours in RNA*later*, samples were frozen at −80°C. RNA was extracted by 3-mm bead beating in Trizol and column purified (Qiagen, Valencia, California). RNA was treated with Ambion Turbo DNA-free DNase (Life Technologies, Grand Island, New York). RNA integrity was assessed using the Agilent 2100 Bioanalyzer (Agilent Technologies, Santa Clara, California), and messenger RNA was enriched using the RIBO-Minus kit (Life Technologies). Successful removal of ribosomal RNA (rRNA) was verified by a second Bioanalyzer assay.

RNA Deep Sequencing

Starting with 200–500 ng of rRNA-depleted total RNA, fragmentation of the whole transcriptome RNA was by chemical induction, as described in Applied Biosystems SOLiD Total RNA-Seq Kit protocol (Applied Biosystems, Carlsbad, California). Fragmented RNA was purified (RiboMinus Concentration Module; Life Technologies), and size distribution and yield were assessed by Bioanalyzer, using the RNA 6000 pico Chip Kit (Agilent Technologies) and Qubit Fluorometer (Life Technologies), respectively. Construction of the amplified whole-transcriptome library was performed as directed in the Applied Biosystems SOLiD Total RNA-Seq Kit protocol. After reverse transcription, each sample was barcoded with a unique 3′ primer during library amplification. Libraries were run on a DNA1000 chip, using the Agilent Bioanalyzer, to assess library size distribution and quality. Quantification of each library was performed by quantitative polymerase chain reaction (qPCR) analysis, and equimolar concentrations of each library were pooled together to proceed with emulsion PCR and sequencing on the AB 5500xl SOLiD sequencer (Applied Biosystems). CTSK expression was verified by real-time PCR. Briefly, RNA was reverse transcribed by a complementary DNA synthesis kit (Agilent, California) with random primers, and real-time PCR was carried out using SYBR green and primers specific for CTSK and β-actin (iQ5 cycler; BioRad, California). Results have been submitted to the gene expression omnibus at the National Center for Biotechnology Innovation (GEO: GSE68206).

Data Analysis

Reads were aligned to the *Oryctolagus cuniculus* genome, using the Bioscope 1.3 Whole Transcriptome Analysis Pipeline (Applied Biosystems, Carlsbad, California). The number of reads mapped to each transcript was calculated using

HTSeq-count v0.5.3. The overlap resolution mode was set to "intersection-nonempty," and the feature type was "exon" (available at: http://www.huber.embl.de/users/anders/HTSeq/doc/install.html#download. Accessed 29 September 2015).

Differential expression was determined using DESeq v1.4.1 (available at: http://genomebiology.com/2010/11/10/R106. Accessed 29 September 2015), using a test based on the negative binomial distribution, modeling both biological and technical variation. *P* values were adjusted for multiple comparisons, using the Benjamini–Hochberg method. Adjusted *P* values of <.05 were considered significant.

Quantification of Collagen Type 1 C-terminal Propeptide (CICP), Helical Peptide, and Deoxypyridinoline (DPD) Levels in Rabbit Urine and Plasma Specimens

CICP, collagen helical peptide, and DPD levels were assessed using enzyme-linked immunosorbent assays (ELISAs; Quidel, San Diego, California). Urinary samples were normalized to creatinine, measured via enzyme immunoassay (Quidel), and plasma samples were normalized to protein (BCA total protein assay, Pierce, Thermoscientific, Rockford, Illinois).

Histologic and Immunohistochemical Staining of Rabbit Samples

Processing was by Histoserv or the Comparative Pathology Core at Johns Hopkins University. Briefly, tissue was dehydrated, embedded in paraffin, cut into 4-μm sections, and stained with hematoxylin-eosin (H-E).

For CTSK immunohistochemical analysis, 5-μm serial sections were washed in xylene, rehydrated and heated by microwave for 20 minutes in unmasking solution (Vector Laboratories, Burlingame, California; reference H-3300). Tissues were incubated for 30 minutes in serum-free protein blocking agent (Dako, Carpinteria, California; reference X0909) and incubated with monoclonal mouse anti-human CTSK primary antibody (AbD Serotec, Oxford, United Kingdom; reference MCA5232Z; 60 minutes) and then with biotinylated goat anti-mouse Fc secondary antibody (30 minutes). The complex was coupled to alkaline phosphatase by biotin and avidin (Vector Laboratories, Burlingame, California; reference AK-5000). The development step used the Vulcan Fast Red chromagen (Biocare, Concord, California; reference FR805) and hematoxylin counterstain. To control for nonspecific signal from secondary antibody binding or chromogen development, we stained serial tissue sections in the absence of primary antibody.

Immunohistochemical Analysis of CTSK in Specimens From Individuals With Cavitary Tuberculosis

Samples from a previously reported study [19] were reassessed by 2 independent pathologists, and the CTSK distribution in acid-fast bacilli–positive samples was defined. Tissues were incubated with mouse monoclonal antibodies to human CTSK (clone 3F9; Abcam, Cambridge, Massachusetts) overnight at 4°C. After washing in PBS, horseradish peroxidase–conjugated secondary antibodies were applied for 1 hour at 37°C, and staining was visualized with 3,3-diaminobenzidine for 2 minutes. Nuclei were counterstained with Mayer's hematoxylin.

Measurement of Plasma Levels of CTSK in Humans

The CTSK concentration in plasma samples stored with ethylenediaminetetraacetic acid were assessed by ELISA (USCN Life Science). Samples were from 12 patients (6 males; median age, 33 years [range, 25–52 years]) with a diagnosis of active pulmonary tuberculosis confirmed by sputum culture and from 10 healthy blood donors (5 males; median age, 30 years [range, 10–58 years]) who were matched for age and sex and recruited between 2012 and 2014. Median MKK values were used as measure of central tendency, and values were compared between the groups using the Mann–Whitney *U* test.

Ethics Statement

Clinical protocols were approved by the institutional review board from the National Institute of Allergy and Infectious Diseases, National Institutes of Health (Bethesda, Maryland; protocol NCT01611402). Animal studies were conducted under approval by the Institutional Animal Care and Use Committee at Johns Hopkins University (protocol RB11M466). These studies were in accordance with the Animal Welfare Act and the Public Health Service Policy. All clinical investigations were conducted according to the Declaration of Helsinki. Written informed consent was obtained from all participants or their legally responsible guardians before subjects enrolled into the study.

RESULTS

Proteases That Cleave Type I Collagen Are Abundantly Expressed in Rabbit Cavity Tissue

A lower-dose sensitizing regimen model was used to generate a range of clinical disease phenotypes in rabbits (Supplementary Figure 1). Three rabbits that developed extensive cavitation as defined by CT were necropsied, and tissue specimens were collected for RNA sequencing. Whole-transcriptome analysis was performed on RNA extracted from 9 samples: 3 from the cavity wall, 3 from grossly normal tissue in the same animals, and 3 from uninfected control animals (Figure 1 and Supplementary Figure 2). Of 17 318 transcripts mapped, expression of 1410 was found to change by >2-fold in the cavity wall, as compared to normal infected tissue (Figure 1*A*), and expression of only 86 protein-coding transcripts changed by >2-fold between normal infected tissue and uninfected tissue (Supplementary Figure 2). A total of 77 protease genes (GO:008 233) were identified among the cavity transcripts (Figure 1*C* and 1*D* and Supplementary Figure 3). Of the 22 proteases that showed significantly different transcription (Figure 1*B* and 1*D*) in cavity and noncavity tissue, 5 are known to cleave fibrillar collagen (Figure 1*C*). These included CTSK, which can cleave both the alpha-1 and alpha-2 subunits of type I collagen; mast cell chymase-1 (CMA1), which cleaves procollagen during initiation of collagen fibril synthesis; as well as MMP-1, MMP-13, and MMP-14.

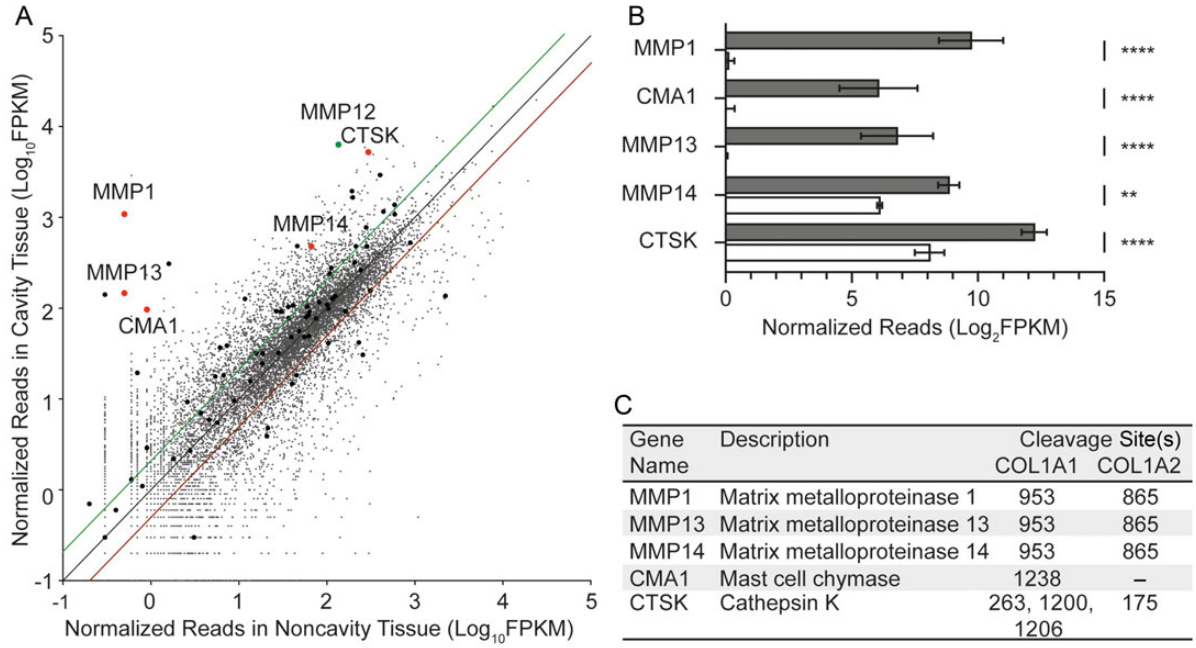

C

Gene Name	Description	Cleavage Site(s) COL1A1	COL1A2
MMP1	Matrix metalloproteinase 1	953	865
MMP13	Matrix metalloproteinase 13	953	865
MMP14	Matrix metalloproteinase 14	953	865
CMA1	Mast cell chymase	1238	–
CTSK	Cathepsin K	263, 1200, 1206	175

D

Gene	Description	Cavity (Log_2FPKM)	Control (Log_2FPKM)	*P*
ACE	Angiotensin I converting enzyme	6.70 ±1.26	11.11 ± 0.27	****
ADAMTS18	A disintegrin-like and metallopeptidase with thrombospondin type 1 motif, 18	4.01 ± 1.05	–0.84 ± 1.62	****
ADAMTSL1	A disintegrin-like and metallopeptidase with thrombospondin type 1 motif-like1	6.23 ± 1.79	3.45 ± 0.64	**
CASP3	Caspase 3	5.21 ± 0.53	2.63 ± 1.10	*
CTSB	Cathepsin B	11.50 ± 0.24	8.61 ± 0.41	**
CTSL	Cathepsin L	10.83 ± 0.61	7.55 ± 0.43	***
CTSS	Cathepsin S	10.65 ± 0.45	7.61 ± 0.24	**
FAP	Fibroblast activation protein, alpha	5.04 ± 0.83	2.56 ± 0.51	*
FOLH1	Folate hydrolase 1	5.26 ± 0.71	7.78 ± 0.56	*
MASP1	Mannose-binding protein associated serine peptidase 1	7.14 ± 0.10	–1.36+/-0.69	**
MME	Membrane metallo-endopeptidase	4.85 ± 0.67	7.93 ± 0.59	**
MMP3	Matrix metalloproteinase 3	7.86 ± 1.39	0.21 ± 1.73	****
MMP12	Matrix metalloproteinase 12	12.38 ± 1.08	7.01 ± 0.60	****
MMP24	Matrix metalloproteinase 24	-1.20 ± 0.99	1.45 ± 0.92	*
PLAU	Plasminogen activator, urokinase	8.76 ± 0.81	5.49 ± 0.42	***
SHH	Sonic hedgehog	1.38 ± 1.59	4.38 ± 0.07	**
UCHL1	Ubiquitin carboxyl-terminal hydrolase	0.64 ± 2.83	4.39 ± 0.36	****

Figure 1. Collagen and collagenase activity are deregulated at the cavity wall, compared with noncavity tissue. *A*, By using RNAseq, 17 318 transcripts (gray dots) were identified in either or both cavity wall (*y*-axis) and infected noncavity tissue (*x*-axis). Seventy-seven proteases (GO:0008322) were identified (larger dots). Levels of transcripts to the left of the green line are 2-fold greater in cavity tissue, compared with noncavity tissue, and levels of transcripts to the right of the red line are 2-fold greater in noncavity tissue, compared with cavity tissue. Five type I collagen–degrading enzymes (as identified by substrate analysis in MEROPS) were identified (red dots). All of these collagenases were significantly upregulated in cavity tissue. Matrix metalloproteinase 12 (MMP12; green dot) was the most abundant protease in cavitary tissue. *B*, Cathepsin K (CTSK) was the most abundant protease capable of cleaving type I collagen. MMP-1, MMP-13, and MMP-14 were significantly upregulated, as was chymase I, which cleaves procollagen during fibril synthesis. *C*, MMP-1, MMP-13, and MMP-14 cleave type I collagen alpha subunits at very specific sites, whereas CTSK can cleave type I collagen at multiple sites. *D*, The remaining upregulated collagenases consisted of other MMP and cathepsin family proteins, but none of these are implicated in physiological degradation of structural collagens. Statistical analysis was performed using 2-way analysis of variance with the Bonferroni post hoc test for comparison within identified proteases. Abbreviation: FPKM, fragments per kilobase of exon per million kilobases mapped.

MMP-12, which can cleave type III collagen, was the most abundantly expressed protease in cavity tissue (Figure 1*A* and 1*D*) [15]. As CTSK has the unique ability to cleave type I collagen both inside and outside the helical domain and has not been previously investigated in tuberculosis, we focused our subsequent studies on this host protease.

CTSK Expression Is Associated With Immunopathology in Rabbits

To confirm and expand upon our sequencing findings, we evaluated a range of lesions from higher-dose sensitization and infected animals for CTSK expression levels by quantitative real-time PCR (Figure 2 and Supplementary Figure 4). Compared with nonpathological tissue, CTSK transcription was

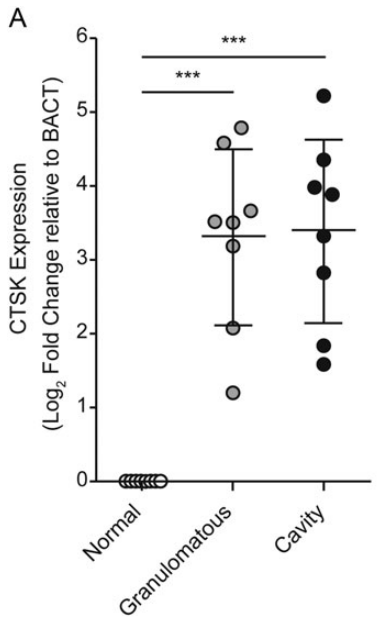

B

Gene	NCBI Reference	Primer Direction	Primer Sequence (5'-3')
CTSK	XM_002711415.1	Forward	ATCGCCAGCGCCACCAAGTT
		Reverse	GCAGCTCCTGCAACTCCTCAA

Sequenced Product (5'-3')
TGGGGACTCAAGGTTCTGCTGCTACCCGTGG TGAGTTTTGCTCT GCACCCTGAGGAAATACTGGACACCCAGTGGGAGCTATGGAAGA AGACCTACAGCAACAGTATAACAGCAAGGTGGATGAAATCTCTCG GCGTTTAATTTGGG

Figure 2. Cathepsin K (CTSK) is expressed in granulomatous and cavitary pathology in a rabbit model that consistently produces human-like pathology, including cavity formation. *A*, Quantitative polymerase chain reaction (qPCR) analysis revealed an increase of >9-fold in *ctsk* expression in granulomatous and cavity tissue, compared with control tissue (n = 8). Data were analyzed by 1-way analysis of variance with the Tukey post hoc comparison test. *B*, Primers used for qPCR and the sequenced product of these primers after qPCR. Abbreviation: NCBI, National Center for Biotechnology Information.

substantially greater, by 9.8-fold, in pathological tissue, both cavitary and granulomatous ($P < .001$; Figure 2). We confirmed the localization of CTSK by performing carefully developed immunohistochemical staining in rabbit pulmonary tissue (Figure 3 and Supplementary Figures 5 and 6). We observed that CTSK protein expression is localized to the periphery of necrotizing, cavitary lesions (Figure 3), within the lesion margins, but not at the necrotic centers (Figure 3*B*–*D*). We also noted that, in small granuloma-like lesions, CTSK was abundantly expressed (Supplementary Figure 5).

Collagen Degradation and Synthesis Are Elevated During Cavitary Tuberculosis

To identify the contribution of collagenases to collagen breakdown in vivo we examined markers of type I collagen breakdown in plasma and urine from animals with a range of clinical manifestations of tuberculosis (Figure 4). Three principal pathologies were defined according to the extent of the cavity (Supplementary Figure 7): (1) cavities that represented immediate risk to the animal's health (terminal cavities; >100 mm^3; these animals became moribund), (2) small cavities were not considered life threatening (nonterminal cavities; all <10 mm^3; these animals were nonmoribund), and (3) noncavitary consolidation (noncavities). We kept animals with nonterminal cavities for prolonged follow-up (Supplementary Figures 8–10). Serum CICP, a marker released during both degradation and synthesis of collagen, was increased by 10-fold ($P = .0193$) in animals with terminal cavities, compared with all other animals (Figure 4*A*). Urinary helical peptide, a marker of degradation that consists of amino acids 620–633 of COL1A1 (alpha-I subunit of type I collagen), was decreased by 3-fold in animals with terminal cavities when compared to the other animals (Figure 4*B*; $P = .0148$). The amount of free urinary DPD, also a marker of degradation, was increased by 4-fold in cavitary animals as compared to noncavitary animals (Figure 4*C*; $P = .068$). Weight change and ^{18}F-FDG uptake did not differ in these animals (Supplementary Figure 8). These data suggested that increased collagen breakdown and resynthesis occurs during cavitation. This was confirmed by examining fibrillar collagen expression (COL1A1, COL1A2, and COL3A1) in cavitary tissue in the sequencing data (Figure 4*D*).

CTSK Is Specifically Expressed in a Circumferential Pattern in Human Tuberculosis Lesions

We next studied CTSK expression in patients with pulmonary tuberculosis. As in the rabbit model, CTSK expression localized to the periphery of lesions (Figure 5 and Supplementary Figure 11) and mononuclear cells at the surface of cavities (Figure 5*A* and 5*B*). Additionally, we observed CTSK expression at the margin of central caseating material and the fibrous cuff (Figure 5*B*). We also confirmed previous observations of abundant CTSK expression in multinucleated giant cells (Figure 5*D*). Finally, we measured levels of CTSK in the plasma of patients with active tuberculosis and compared levels to those in healthy controls. Mean CTSK levels were 13-fold greater ($P = .0013$) in the peripheral circulation of patients with active tuberculosis, compared with healthy controls (Figure 6).

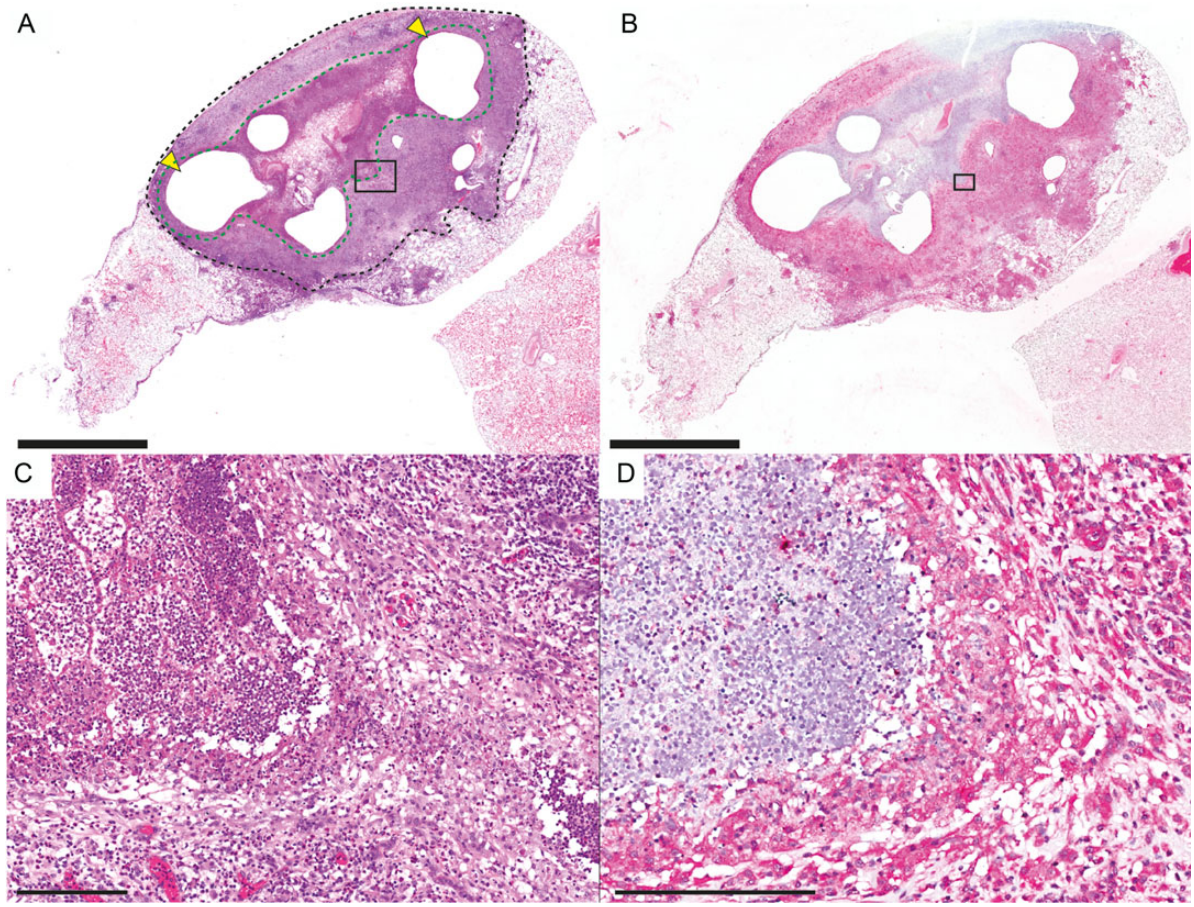

Figure 3. Cathepsin K (CTSK) is expressed in nonnecrotic regions of cavitary lesions. CTSK expression in rabbit pulmonary lesions as assessed by immunohistochemical analysis (*B* and *D*), compared with hematoxylin-eosin (H-E)–stained sections (*A* and *C*). *A*, H-E–stained section demonstrating a large caseous lesion (green dotted line) with regions of early cavitation (yellow arrows), surrounded by lipoid pneumonia (black dotted line). *B*, Red anti-CTSK staining localized to the region of lipoid pneumonia. *C*, Enlarged region showing both necrotic tissue and the adjacent mononuclear infiltrate and lipoid pneumonia. *D*, CTSK was expressed primarily in the mononuclear infiltrate and occasionally in cells infiltrating the necrotic debris. Thick bars, 5 mm; thin bars, 200 μM.

DISCUSSION

Tuberculosis continues to plague humankind, and the increasing burden of antibiotic-resistant disease is forcing a return to low-potency, toxic therapeutic regimens [20]. These regimens are extremely costly and have limited efficacy [20]. By dissecting the destructive and protective components of the host immune response, appropriately targeted host-directed therapies may restore immune function and facilitate antibiotic efficacy or offer novel therapeutic advantages in resistant disease [21].

Type I collagen is the key structural component of lung tissue and is distributed throughout the distensible lung regions and provides the mechanical scaffold, while type III collagen is the principal component of alveolar walls [22]. The role of collagen extends beyond the mechanical, facilitating cellular polarity, immune activation, and cellular migration [22]. Collagen degradation in the lung is currently irreversible, and it is typically followed by fibrotic scarring that impairs functionality [22, 23]. Because of this, ECM degradation is tightly regulated [22]. In tuberculosis, extensive fibrosis develops around cavities, which usually persists even after cure of infection, resulting in significantly impaired lung function [24]. In our study, we demonstrated upregulation of multiple collagens and the formation of thick-walled cavities in rabbits, further demonstrating that, in tuberculosis, the matrix remodeling that occurs is dysregulated and obliterates the normal microarchitecture of the lung. Further studies will be required to determine whether earlier prevention of lung destruction by protease inhibition will reduce subsequent fibrosis and impairment of lung function.

We demonstrated that type I collagen cleavage is a feature of cavitation, in agreement with a previous hypothesis regarding cavity formation in pulmonary disease [25]. We identified that CTSK was the most abundantly expressed protease capable of type I collagen cleavage, with levels greater than MMP-1, a collagenase associated with active tuberculosis in multiple cohorts [26–28]. In humans with tuberculosis, CTSK was

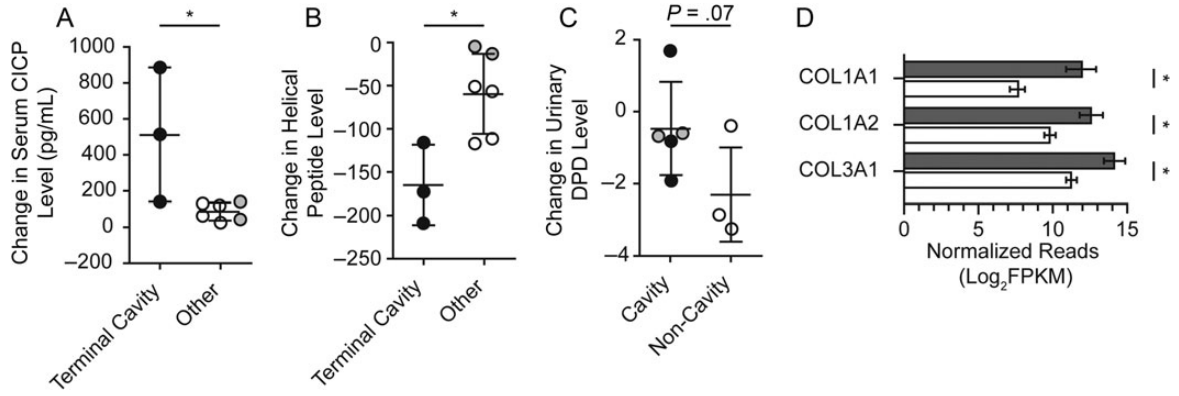

Figure 4. Collagen metabolites vary with disease phenotype in the rabbit model. *A*, The level of C-propeptide of type I procollagen (CICP) in serum was measured at the time of cavitation (day 21) and compared to day 0 serum CICP levels. An increase in CICP level was seen in all infected animals, but this increase was significantly greater in animals with terminal cavities, compared with those without. *B*, A decrease in the level of urinary helical peptide, a fragment of COL1A1, was observed in all infected animals when urine specimens obtained on day 21 were compared to those obtained on day 0 but was lower in animals with terminal cavities. *C*, The level of urinary deoxypyridinoline (DPD) did not change significantly with infection, and there was an insignificant reduction in the level of DPD in animals that did not cavitate. *D*, Fibrillar collagen expression was significantly increased in cavity wall tissue. Expression of all components of type I collagen (COL1A1 and COL1A2) and type III collagen (COL3A1) was increased, as analyzed by RNAseq.

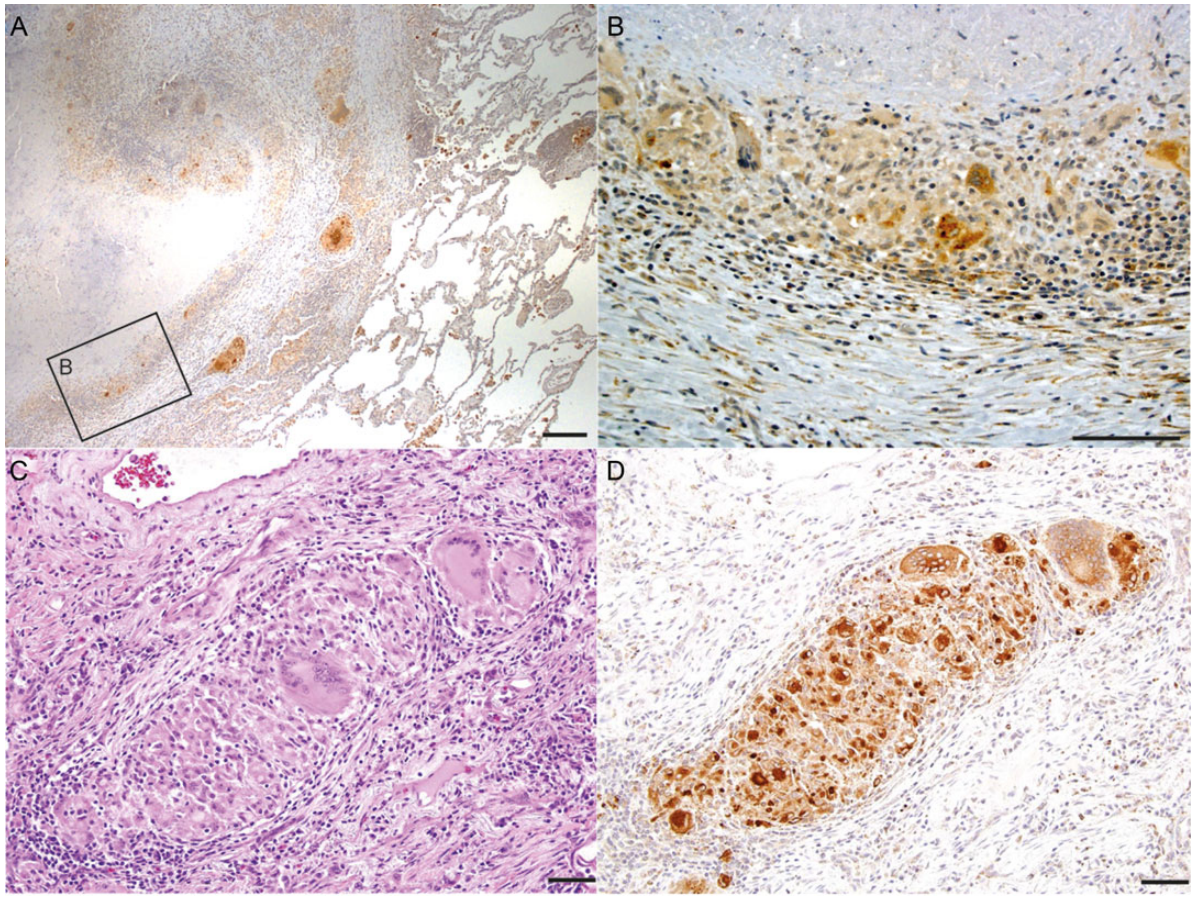

Figure 5 Cathepsin K (CTSK) is abundant in human pulmonary tuberculosis lesions. *A*, A section stained with anti-CTSK antibody. CTSK is mainly localized at the periphery of the small granulomas and in the material abutting the cavity. *B*, Magnified view demonstrating CTSK staining in monocytes in the fibrous cuff of the granuloma. There is also immunoreactivity in the fibroblast-like cells within the fibrous layer. *C*, A hematoxylin-eosin (H-E)–stained section demonstrating an encapsulated granuloma with multinucleated giant cells. *D*, An anti-CTSK–stained section adjacent to section in panel *C*, demonstrating abundant CTSK expression within the multinucleated giant cells. Scale bars: 1 mm (*A*) and 200 μm (*B*–*D*).

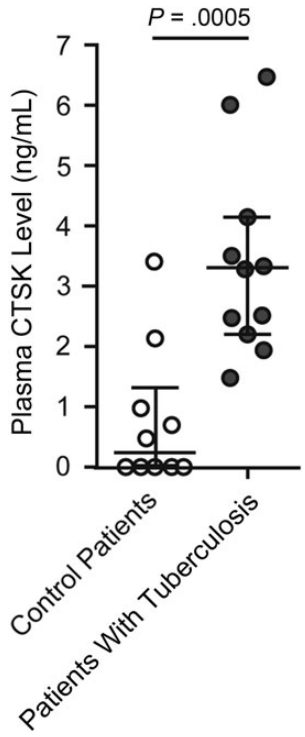

Figure 6. Cathepsin K (CTSK) expression is elevated in the plasma of patients with tuberculosis. Plasma concentrations of CTSK in patients with active tuberculosis are 13-fold greater than those in matched uninfected controls. The *P* value was calculated, by the Mann–Whitney *U* exact test.

expressed not only by cells within granulomatous tissue, but levels were also significantly elevated in plasma. The localization of CTSK to the mononuclear infiltrate suggests that these monocytes are of a tissue-degrading phenotype [29, 30].

We show that changes in urinary and serum markers of collagen metabolism correlate with cavity formation, indicating both synthetic and collagenolytic processes and a role for non-MMP–mediated type I collagen degradation. Our data do not indicate how these pathways are regulated; transforming growth factor β, a central mediator of fibrosis, was not mapped in our sequencing data. ECM synthesis is commonly the result of fibroblastic activity, and in more mature lesions there is clear evidence of poorly stained fibrotic regions and cells with fibroblastic morphology in the rabbit cavity wall [13]. Further studies of the regulatory mechanisms are clearly warranted, as these may represent targets for host-directed therapies in tuberculosis and also reveal mechanistic processes underlying other fibrotic lung diseases [31, 32].

In this study, we specifically investigated components of type I collagen because, of the 23 significantly upregulated proteases, 5 type I collagenases were identified. Levels of CICP, a collagen peptide released during fibril formation and destruction, were increased in cavitary animals. Our results are consistent with the observation that PIIINP levels (a marker of type III collagen turnover) are increased in active tuberculosis [33]. MMP-1, MMP-13, and MMP-14 are known to be upregulated in rabbit cavitary tissue [13], an observation confirmed in our sequencing data (Figure 1*B*) and correlative with findings from human studies [26–28]. We found macrophage elastase MMP-12 to be highly expressed and upregulated in cavity tissue, although the significance of this finding is unclear as MMP-12 is not induced in human tuberculosis [26, 34]. MMP-1, MMP-13, and MMP-14 all cleave collagen at a unique site located at amino acid 953 (Figure 1*C*) [15, 35]. The reduction in helical peptide levels that we observed suggest that this fragment is being degraded and indicates that collagen is cleaved outside of the helical region during active tuberculosis. These findings suggested a previously unidentified role for non-MMP collagenolysis in active tuberculosis, implicating CTSK.

Regulators of ECM remodeling, including pirfenidone, nintedanib, odanacatib, and mongersen, are entering the clinical arena [36–39]. Our understanding of these drugs' effects on ECM-related immune function remains limited. Our data suggest that ECM degradation is a key component of active tuberculosis and, therefore, that these drugs, as well as more-specific MMP and CTSK inhibitors, such as odanacatib, cipemastat, and doxycycline [17, 26, 27, 40], may affect immune balances in pulmonary pathologies [41]. Further study of the role of matrix degradation as a key contributor and potential therapeutic target is warranted, given the potential to repurpose this growing arsenal of drugs to treat destructive pulmonary pathologies. Clearly, caution must be taken if we are to manipulate ECM turnover in the context of infection, as it is known to play a role in immune cell function and cellular migration [42, 43].

Tuberculin skin test (TST) positivity predicted cavity formation in our model (Figure 4*B*) and is associated with excessive collagenase activity in our model. We did not demonstrate an association between TST reactivity and cavity size, although this may reflect a lack of power due to the sample size or alternatively the inherent variability of outbred rabbits. Prolonged follow-up of our animals revealed that animals that developed cavities were more likely to have progressive active disease (as defined by ^{18}F-FDG PET scanning) than those without (Supplementary Figures 9 and 10). However, ^{18}F-FDG uptake did not predict bacterial burden (Supplementary Figure 12). This suggests a significant role for immune activity, rather than bacterial burden, in driving active disease.

In summary, we investigated cavitary disease, revealing that collagenolytic enzyme expression and collagen turnover are key components of cavitation in a rabbit model of tuberculosis. We identified a role for CTSK in the immunopathogenesis of cavitary tuberculosis in animals and showed correlative findings in humans. Collagenolysis is not known to be a functional component of any immune response, and so there is a possibility that inhibition of this process may benefit the host without

adversely affecting immune control of bacterial replication. Further experiments to see whether targeting CTSK can prevent cavitation without inhibiting tissue repair are required. The postprimary rabbit model provides an optimal system for such investigations, and the investigation of other therapeutics that modulate extracellular matrix degradation [13, 44]. Such studies will have the dual benefit of assisting our understanding of the importance of matrix regulation in immune responses, as well as providing an avenue, if justified, to bring these therapeutic agents to the clinic.

Supplementary Data

Supplementary materials are available at http://jid.oxfordjournals.org. Consisting of data provided by the author to benefit the reader, the posted materials are not copyedited and are the sole responsibility of the author, so questions or comments should be addressed to the author.

Notes

Acknowledgments. We thank Dr Irini Sereti (NIAID, NIH) for providing the serum samples from patients with tuberculosis.

A. K., B. L., C. L., N. C. A., L. S. C., and K. W. designed and performed the animal experiments. A. K., B. L., C. L., M. U., and K. W. designed and conducted RNA analysis. B. B. A., M. O., K. B., M. H., and J. K. P. developed, designed, performed, and interpreted the histopathological assessment of rabbit and human tissues. E. P. A. and B. B. A. designed and performed human serum collection and analysis. A. S., J. S. F., P. T. E., and W. R. B. contributed to study design, manuscript preparation, and grant acquisition. All authors reviewed and contributed to manuscript preparation.

Disclaimer. The content of this publication does not necessarily reflect the views or policies of the Department of Health and Human Services, nor does mention of trade names, commercial products, or organizations imply endorsement by the US government. The sponsor had no role in the design of the study, the collection and analysis of the data, or the preparation of the manuscript.

Financial support. This work was supported by the Howard Hughes Medical Institute (to W. R. B.), the National Institutes of Health (NIH; R01 AI 079590, R01 AI037856, and R01 AI036973 to W. R. B. and R33 A1102239 to P. E.), the NIH Intramural Research Program (to A. S., B. B. A., and E. P. A.), Imperial College London (to A. K. and J. S. F.), the Swedish Research Council (to C. L.), and the Swedish Society for Medical Research (to C. L.).

Potential conflicts of interest. All authors: No reported conflicts. All authors have submitted the ICMJE Form for Disclosure of Potential Conflicts of Interest. Conflicts that the editors consider relevant to the content of the manuscript have been disclosed.

References

1. Tiemersma EW, van der Werf MJ, Borgdorff MW, Williams BG, Nagelkerke NJD. Natural history of tuberculosis: duration and fatality of untreated pulmonary tuberculosis in HIV negative patients: a systematic review. PLoS One **2011**; 6:e17601.
2. Marks SM, Flood J, Seaworth B, et al. Treatment practices, outcomes, and costs of multidrug-resistant and extensively drug-resistant tuberculosis, United States, 2005–2007. Emerg Infect Dis **2014**; 20:812–21.
3. Canetti G. The tubercle bacillus in the pulmonary lesion of man; histobacteriology and its bearing on the therapy of pulmonary tuberculosis. American rev. ed. New York: Springer, **1955**.
4. Golub JE, Bur S, Cronin WA, et al. Delayed tuberculosis diagnosis and tuberculosis transmission. Int J Tuberc Lung Dis **2006**; 10:24–30.
5. Visser ME, Stead MC, Walzl G, et al. Baseline predictors of sputum culture conversion in pulmonary tuberculosis: importance of cavities, smoking, time to detection and W-Beijing genotype. PLoS One **2012**; 7:e29588.
6. Kim HR, Hwang SS, Kim HJ, et al. Impact of extensive drug resistance on treatment outcomes in non-HIV-infected patients with multidrug-resistant tuberculosis. Clin Infect Dis **2007**; 45:1290–5.
7. Dannenberg AM. Pathogenesis of human pulmonary tuberculosis : insights from the rabbit model. Washington, DC: ASM Press, **2006**.
8. Robbins SL, Kumar V, Cotran RS. Robbins and Cotran pathologic basis of disease. 8th ed. Philadelphia, PA: Saunders/Elsevier, **2010**.
9. Lenaerts A, Barry CE, Dartois V. Heterogeneity in tuberculosis pathology, microenvironments and therapeutic responses. Immunol Rev **2015**; 264: 288–307.
10. Russell DG. Who puts the tubercle in tuberculosis? Nat Rev Microbiol **2007**; 5:39–47.
11. Gadkowski LB, Stout JE. Cavitary pulmonary disease. Clin Microbiol Rev **2008**; 21:305–33.
12. Hunter RL. Pathology of post primary tuberculosis of the lung: an illustrated critical review. Tuberculosis **2011**; 91:497–509.
13. Kubler A, Luna B, Larsson C, et al. *Mycobacterium tuberculosis* dysregulates MMP/TIMP balance to drive rapid cavitation and unrestrained bacterial proliferation. J Pathol **2014**; 235:431–44.
14. Price AP, England KA, Matson AM, Blazar BR, Panoskaltsis-Mortari A. Development of a decellularized lung bioreactor system for bioengineering the lung: the matrix reloaded. Tissue Eng Part A **2010**; 16:2581–91.
15. Rawlings ND, Waller M, Barrett AJ, Bateman A. MEROPS: the database of proteolytic enzymes, their substrates and inhibitors. Nucleic Acids Res **2014**; 42: D503–9.
16. Chang S-W, Buehler MJ. Molecular biomechanics of collagen molecules. Mater Today **2014**; 17:70–6.
17. Brömme D, Okamoto K, Wang BB, Biroc S. Human cathepsin O2, a matrix protein-degrading cysteine protease expressed in osteoclasts. J Biol Chem **1996**; 271:2126–32.
18. Kesavan AK, Mendez SE, Hatem CL, et al. Effects of dexamethasone and transient malnutrition on rabbits infected with aerosolized *Mycobacterium tuberculosis* CDC1551. Infect Immun **2005**; 73:7056–60.
19. Park JK, Rosen A, Saffitz JE, et al. Expression of cathepsin K and tartrate-resistant acid phosphatase is not confined to osteoclasts but is a general feature of multinucleated giant cells: systematic analysis. Rheumatology **2013**; 52:1529–33.
20. World Health Organization. Global tuberculosis report 2013. Geneva: WHO, **2013**.
21. Hawn TR, Matheson AI, Maley SN, Vandal O. Host-directed therapeutics for tuberculosis: can we harness the host? Microbiol Mol Biol Rev **2013**; 77: 608–27.
22. Davidson JM. Biochemistry and turnover of lung interstitium. Eur Respir J **1990**; 3:1048–63.
23. Zeisberg M, Kalluri R. Cellular mechanisms of tissue fibrosis. 1. Common and organ-specific mechanisms associated with tissue fibrosis. Am J Physiol Cell Physiol **2013**; 304:C216–25.
24. Rhee CK, Yoo KH, Lee JH, et al. Clinical characteristics of patients with tuberculosis-destroyed lung. Int J Tuberc Lung Dis **2013**; 17:67–75.
25. Elkington PT, Armiento JM, Friedland JS. Tuberculosis immunopathology: the neglected role of extracellular matrix destruction. Sci Transl Med **2011**; 3:71ps6.
26. Elkington P, Shiomi T, Breen R, et al. MMP-1 drives immunopathology in human tuberculosis and transgenic mice. J Clin Invest **2011**; 121:1827–33.
27. Walker NF, Clark SO, Oni T, et al. Doxycycline and HIV infection suppress tuberculosis-induced matrix metalloproteinases. Am J Respir Crit Care Med **2012**; 185:989–97.
28. Ugarte-Gil CA, Elkington P, Gilman RH, et al. Induced sputum MMP-1, -3 & -8 concentrations during treatment of tuberculosis. PLoS One **2013**; 8:e61333.
29. Buhling F, Reisenauer A, Gerber A, et al. Cathepsin K–a marker of macrophage differentiation? J Pathol **2001**; 195:375–82.
30. Park JK, Askin F, Giles JT, Halushka MK, Rosen A, Levine SM. Increased generation of TRAP expressing multinucleated giant cells in patients with granulomatosis with polyangiitis. PLoS One **2012**; 7:e42659.
31. Spagnolo P, Del Giovane C, Luppi F, et al. Non-steroid agents for idiopathic pulmonary fibrosis. Cochrane Database Syst Rev **2010**; doi:10.1002/14651858.CD003134.pub2.
32. Zumla A, Chakaya J, Hoelscher M, et al. Towards host-directed therapies for tuberculosis. Nat Rev Drug Discov **2015**; 14:511–2.
33. Seddon J, Kasprowicz V, Walker NF, et al. Procollagen III N-terminal propeptide and desmosine are released by matrix destruction in pulmonary tuberculosis. J Infect Dis **2013**; 208:1571–9.
34. Kahnert A, Seiler P, Stein M, et al. Alternative activation deprives macrophages of a coordinated defense program to *Mycobacterium tuberculosis*. Eur J Immunol **2006**; 36:631–47.
35. Manka SW, Carafoli F, Visse R, et al. Structural insights into triple-helical collagen cleavage by matrix metalloproteinase 1. Proc Natl Acad Sci U S A **2012**; 109: 12461–6.

36. King TE Jr, Bradford WZ, Castro-Bernardini S, et al. A phase 3 trial of pirfenidone in patients with idiopathic pulmonary fibrosis. N Engl J Med **2014**; 370: 2083–92.
37. Richeldi L, du Bois RM, Raghu G, et al. Efficacy and safety of nintedanib in idiopathic pulmonary fibrosis. N Engl J Med **2014**; 370:2071–82.
38. Bone HG, Dempster DW, Eisman JA, et al. Odanacatib for the treatment of postmenopausal osteoporosis: development history and design and participant characteristics of LOFT, the Long-Term Odanacatib Fracture Trial. Osteoporos Int **2015**; 26:699–712.
39. Monteleone G, Neurath MF, Ardizzone S, et al. Mongersen, an oral SMAD7 antisense oligonucleotide, and Crohn's disease. N Engl J Med **2015**; 372:1104–13.
40. Langdahl B, Binkley N, Bone H, et al. Odanacatib in the treatment of postmenopausal women with low bone mineral density: Five years of continued therapy in a phase 2 study. J Bone Miner Res **2012**; 27:2251–8.
41. Al Shammari B, Shiomi T, Tezera L, et al. The extracellular matrix regulates granuloma necrosis in tuberculosis. J Infect Dis **2015**; 212:463–73.
42. Parks WC, Shapiro SD. Matrix metalloproteinases in lung biology. Respir Res **2001**; 2:10–9.
43. Nagase H, Visse R, Murphy G. Structure and function of matrix metalloproteinases and TIMPs. Cardiovasc Res **2006**; 69:562–73.
44. Luna B, Kubler A, Larsson C, et al. In vivo prediction of tuberculosis cavity formation in rabbits. J Infect Dis **2014**; 211:481–5.